*International Journal of Geographical Information Science*
Vol. 19, No. 10, November 2005, 1131–1147



**Research Article**

# Marine GIS: Identification of mesoscale oceanic thermal fronts

V. D. VALAVANIS*†, I. KATARA‡ and A. PALIALEXIS‡

†National Centre for Marine Research, Institute of Marine Biological Resources, Marine GIS Lab, PO Box 2214, 71003 Iraklion Crete, Greece

‡University of Crete, Department of Biology, PO Box 2208, 71409 Iraklion Crete, Greece

(*Received 13 January 2005; in final form 10 March 2005*)

A new method (the 'sink' method) is proposed for the mapping of productive mesoscale oceanic thermal fronts based on the combined analysis of satellite imagery for sea surface temperature (SST) distribution and chlorophyll (CHL) concentration under a Geographic Information System (GIS). In an SST lattice data array, data value sinks describe heterogeneous drops in SST distribution as this is compared to more homogeneously distributed SST in the surrounding area. Using Arc/Info GIS, these thermal discontinuities are flagged and applied on SST and CHL imagery for the calculation of differences in SST and CHL patterns (DSST and DCHL) inside and outside of these flagged areas. Spatially connected sinks that are characterized by simultaneous negative DSST and positive DCHL pattern are mapped as thermal fronts. Results include a time series of monthly front occurrence GIS maps in Eastern Mediterranean waters along with three calculated front characteristics (DSST, DCHL and bathymetry). Comparisons between the mapped fronts and isobath distributions present clearly visible front-to-isobath spatial and shape associations while spatial analysis between front and wind data explains 66% of the number of mapped fronts.

*Keywords*: Ocean process; Remote sensing; AVHRR; SeaWiFS; Fisheries

## 1. Introduction

Fronts in the ocean are regions of rapid change in salinity or temperature defining the boundary between water masses of different origin. Oceanic fronts can be permanent large-scale features (e.g. Gulf Stream front and Kuroshio Current front) or transient mesoscale features usually occurring seasonally with more diffuse boundaries.

Thermal fronts are zones with a pronounced horizontal temperature gradient, often associated with high productivity levels. When water masses of different origin converge, nutrients as well as phytoplankton and zooplankton are trapped in their convergence zone and productivity increases. In a mesoscale transient pattern, thermal fronts are related to heterogeneous drops in temperature distribution as this is compared to more homogeneous temperature distribution in the surrounding area. These wind-driven and bottom topography-aided productive ocean processes may only appear in the ocean for a few weeks or months during the year, but they

*Corresponding author. Email: vasilis@her.hcmr.gr

*International Journal of Geographical Information Science*
ISSN 1365-8816 print/ISSN 1362-3087 online © 2005 Taylor & Francis
http://www.tandf.co.uk/journals
DOI: 10.1080/13658810500391206

are an important component of the ocean system in sub-basin scale from both physical (Agostini and Bakun 2002) and biological (Malakoff 2004) perspectives.

During the last two decades, the use of environmental satellites has greatly improved our ability to study the characteristics of ocean fronts. With the availability of satellite data, the unique signature of fronts is now identifiable in the gradients of sea surface temperature (SST), height and colour imagery (Belkin 2002, Legeckis *et al*. 2002). In satellite images with adequate resolution to give measurable effect of mesoscale temperature and chlorophyll (CHL) heterogeneity, these processes are shown as linear features in more homogeneous and undisturbed distribution in the surrounding region. Many studies utilize time series of satellite data for the identification and mapping of oceanic fronts in the world oceans (Cayula and Cornillon 1992, 1995, Belkin and Gordon 1996, Ferrier and Anderson 1997, Bonatti and Rao 1999, Ullman and Cornillon 1999, Hickox *et al*. 2000, Mavor and Bisagni 2001, Ullman and Cornillon 2001, Valavanis 2002, Acha *et al*. 2004, Kostianoy *et al*. 2004, Miller 2004). In the Western Mediterranean basin several authors reported relations between physical and biological interactions in fronts (Allen *et al*. 2001, Fielding *et al*. 2001, L'Helguen *et al*. 2002, Sabates *et al*. 2004), while in Central and Eastern Mediterranean, any information on front occurrence is inferred from studies of other oceanographic features (Feliks and Ghil 1993, Borzelli and Ligi 1999, Velegrakis *et al*. 1999, Nardelli *et al*. 2001, Valavanis *et al*. 2004).

A limited number of studies utilize Geographic Information System (GIS) technology to analyse remotely sensed data for the mapping of oceanic fronts. Mesick *et al*. (1998) and Waluda *et al*. (2001) used GIS to apply certain temperature gradients to SST images, while Valavanis (2002) used GIS to map ocean fronts as boundaries of persistent environmental anomaly patterns derived from time series of SST images. Ullman and Cornillon (2000) evaluated the two main methods of using SST satellite data for automated edge-detection of fronts, the histogram and the gradient algorithm methods, and reported that missed-front error rates depend on image threshold values and spatial scales of fronts. They suggest that frontal climatologies developed from the application of automated edge-detection methods to long time series of SST images provide acceptably accurate statistics on front occurrence. On the other hand, Shaw and Vennell (2000) suggest a front-following algorithm for a time series of SST imagery, integrating physical parameters of fronts (not included in edge-detection methods) such as mean temperature, width, and temperature difference across the front with successful application on the mapping of the permanent Subtropical Front in the southwest Pacific Ocean (Shaw and Vennell 2001).

This work proposes a different approach of using satellite data for the identification of mesoscale transient thermal fronts. We perceive transient thermal fronts as data value sinks in an SST lattice data array and we consider these sinks as heterogeneous drops in SST distribution as this is compared to more homogeneously distributed SST in the surrounding area. We utilize a GIS to flag sink cells in SST grids, extract sink-cell environmental information from SST and CHL images and identify the location of productive thermal fronts. We combine station wind and front data to explain the causal effect of these thermal discontinuities. Finally, we use bathymetry data to show significant spatial associations of mapped fronts to certain topographic features.

## 2. Data and methods

The study area is located in the Eastern Mediterranean Sea, including the Hellenic Seas (34°N, 19°E and 42°N, 30°E) comprising four main water bodies, the Aegean and Ionian Seas, and the northern parts of the Libyan and Levantine Seas (see figure 1). The topography of the area is characterized by extreme changes in bathymetry, featuring extensive shallow continental shelves (North Aegean and Cyclades Plateau) interrupted by deep trenches (North Aegean trough, and Chios and Cretan basins). The oceanography of the area is influenced by nutrient-rich waters through river and Black Sea input (North Aegean Sea), and by the northward Asia Minor Current (northern part of the Levantine Sea). The whole area is influenced by strong northwesterly Etesian winds that blow during summer, causing productive upwelling along the east coast of the Aegean Sea and establishing two main homogeneously stratified water bodies divided by an east-to-west temperature gradient along the central Aegean Sea with colder temperatures in the east and warmer temperatures in the west. During winter (no Etesians), an overall cyclonic surface circulation is established with a northerly current along the Asia Minor coast and a southerly current along the Greek coast creating heterogeneous water stratification patterns.

Satellite imagery on SST, obtained from the Advanced Very High Resolution Radiometer (AVHRR) is used for the identification of thermal fronts. A time-series of monthly AVHRR SST imagery was downloaded from the Deutschen Zentrum fur Luft- und Raumfahrt (DLR-German Aerospace Agency) online satellite data archive using DLR's Graphical Interface to the Intelligent Satellite Data Information System (GISIS). Satellite images on sea surface CHL, obtained from

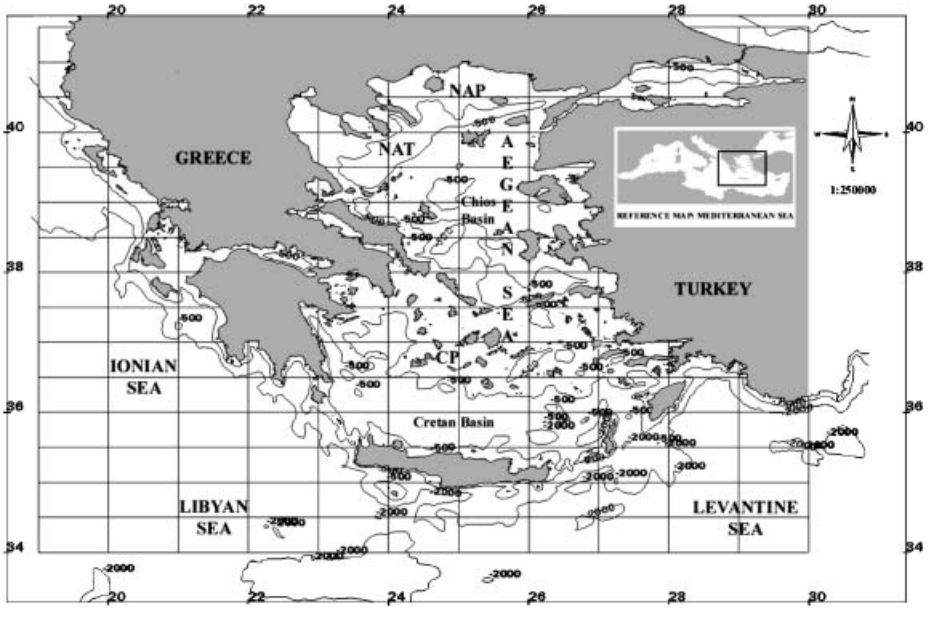


Figure 1. Hellenic Seas: the study area is located in the Eastern Mediterranean Sea, including the Aegean Sea and part of the Ionian, Libyan and Levantine Seas as well as the North Aegean Plateau (NAP) and Cyclades Plateau (CP) interrupted by the North Aegean Trough (NAT) and the Chios and Cretan Basins. Bathymetric contours of 500 m and 2000 m are also shown.

the Sea-viewing Wide Field-of-view Sensor (SeaWiFS), were downloaded from the National Aeronautics and Space Administration's Distributed Active Archive Centre (NASA-DAAC) using the DAAC's online data dissemination interactive hierarchical system. Both satellite datasets were georeferenced and converted to regular grids using Environmental Systems Research Institute (ESRI) Arc/Info GRID GIS. Daily station wind force data (maximum sustained wind speed) were downloaded from the National Oceanic and Atmospheric Administration's National Climatic Data Centre (NOAA-NCDC) online archive in text files and were averaged on a monthly basis and inserted into GIS as monthly station point measurements. Satellite data cover the Hellenic Seas with a temporal resolution 01/1998 to 12/2003 and adequate 1.3 km (SST) and 1.1 km (CHL) spatial resolution while wind station data cover the north part of the study area (North Aegean Sea). There is a 6-month missing data period for SST imagery (10/2001 to 03/2002). Bathymetric contours were derived from extensive sampling of multi-beam bathymetry data obtained from research vessel surveys of the Hellenic Centre for Marine Research (HCMR) during the last two decades.

The identification and mapping of mesoscale thermal fronts are based on ESRI's Arc/Info GRID GIS (version 8.0.2), while data analysis routines are developed in AML (Arc Macro Language, ESRI 1994). The developed AML is compatible with the latest version of ESRI ArcGIS product. The AVHRR SST grid is considered as a uniform lattice data type array of 'elevation' values (orthogonal grid with constant spacing in each direction), while front areas are considered as sinks of SST values in the lattice data array (thermal discontinuities). Sink areas are sets of spatially connected cells whose flow direction out of each cell cannot be determined. These cells describe areas of heterogeneous drop in SST distribution as this is compared to more homogeneous SST distribution in the surrounding area (see figure 2(A)). The computation of flow is based on a $3 \times 3$ window algorithm that assigns specific out-of-cell flow direction values for each cell based on the SST values of its eight neighbouring cells. A sink is a cell or set of spatially connected cells whose flow direction cannot be assigned one of the eight valid values in a flow direction grid. This can occur when values in all neighbouring cells are higher than that of the processing cell or when two cells flow into each other. Sinks are considered to have undefined flow direction and are assigned a value that is the sum of their possible directions. For example (see figure 2(B)), if the steepest drop, and therefore flow direction, is the same both to the right (1) and left (16), the value 17 would be assigned as the flow direction for that cell. Then, cells with undefined flow direction (cells flagged as sinks) are selected from the flow direction grid and converted to lines using a vectorization routine (raster/vector conversion) that eliminates one-cell sinks converting to vectors only spatially connected sink cells (see figure 2(C)).

The calculation of SST difference (DSST) between spatially connected sink cells and their surrounding area is computed by subtracting the SST values of sink-neighbouring area from those of the sink cells. Accordingly, the mapped sinks (derived from the SST grids) are used on the CHL grids to compute the CHL difference (DCHL) between the sink cells and their surrounding area. In both SST and CHL images, the surrounding area of sink cells is defined by a buffer of five cells in all directions around the sink cells. Mapped sinks that are characterized by any combination of DSST and DCHL other than $DSST<0$ and $DCHL>0$ are considered as simple cold-water patches and eliminated. Only those mapped sink

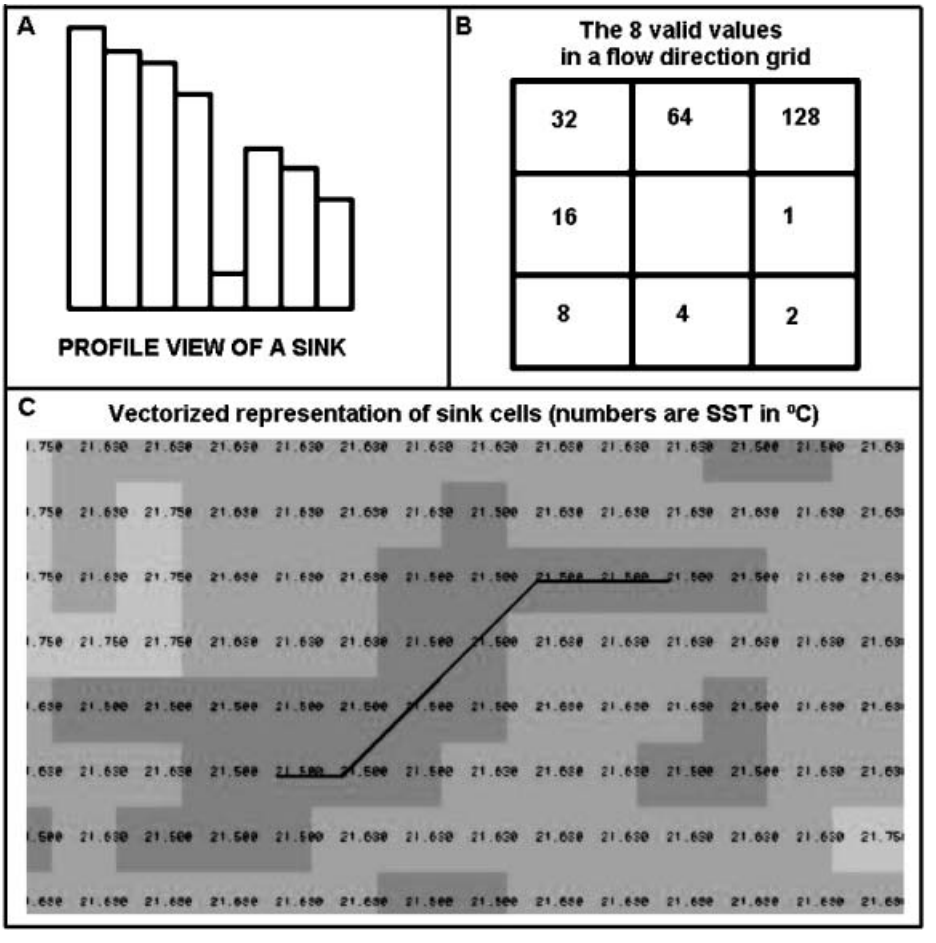


Figure 2. A graphical description of the 'sink' method for the mapping of mesoscale oceanic thermal fronts is shown. (A) Perspective view of thermal fronts in an AVHRR SST lattice data array; fronts are considered as data sinks in more homogeneously distributed SST data. (B) The eight valid values in an SST flow direction grid. Sinks are pixels with undefined flow direction and are assigned values other than those of the eight valid values in the flow direction grid. (C) A mapped front (black line) derived from flagged thermal discontinuity pixels in an SST image using the 'sink' method.

areas that are characterized by simultaneous DSST$<$0 and DCHL$>$0 patterns are mapped as mesoscale thermal fronts.

In order to examine the causal effect of the observed productive thermal discontinuities, we used S-Plus 2000 (MathSoft 1999) to develop a Spearman's correlation (method based on data ranks and not so sensitive to outliers) and a linear regression model between the variability of maximum sustained wind speed (in terms of standard deviation) and the number of mapped fronts in the North Aegean Sea. A time series analysis was applied on derived front characteristics (monthly DSST and DCHL and bathymetry) in order to identify seasonal patterns. The analysis includes autocorrelations, periodograms and seasonal decomposition (additive method). The Kruskall-Wallis test and corresponding Box-Whisker plots were used for the comparison between the properties of shelf, shelf break and open water fronts.

## 3. Results and discussion

A selected subset of our results is presented here. The overall results include 66 monthly, 18 seasonal and six yearly images of mesoscale thermal fronts covering the Hellenic Seas for the period 01/1998 to 12/2003 (missing data period: 10/2001 to 03/2002) and they are available online at: arch.imbc.gr. Selected months of mapped mesoscale thermal fronts are presented along with bathymetric contours in three marine areas that sustain most of the fisheries' production in the Hellenic Seas, the North Aegean Sea (see figure 3), the South Cretan Sea (see figure 4) and the North Ionian Sea (see figure 5). Yearly mapped fronts on shaded bathymetry are presented in the North Aegean Sea for 1998 (see figure 6). In addition, mapped fronts are presented in relation to wind data (see figure 7) while calculated characteristics of mapped thermal fronts are presented in Table 1.

Distribution relations of mapped thermal fronts to bathymetry and wind patterns are encouraging. Identified fronts are clearly related to bathymetric contours and often, the shape of fronts is similar to the shape of the associated isobath.

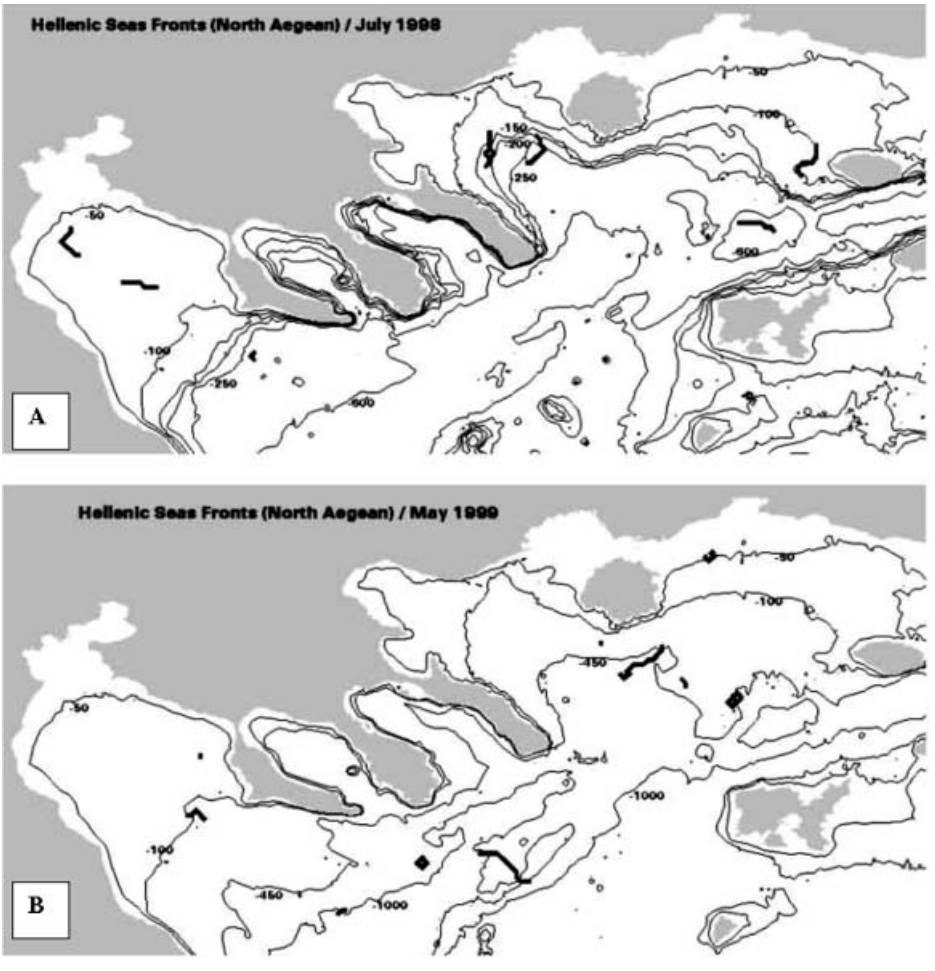


Figure 3. Front and isobath associations in the North Aegean Sea in (A) July 1998 and (B) May 1999. Spatial and shape associations are clearly visible along a wide bathymetric range.

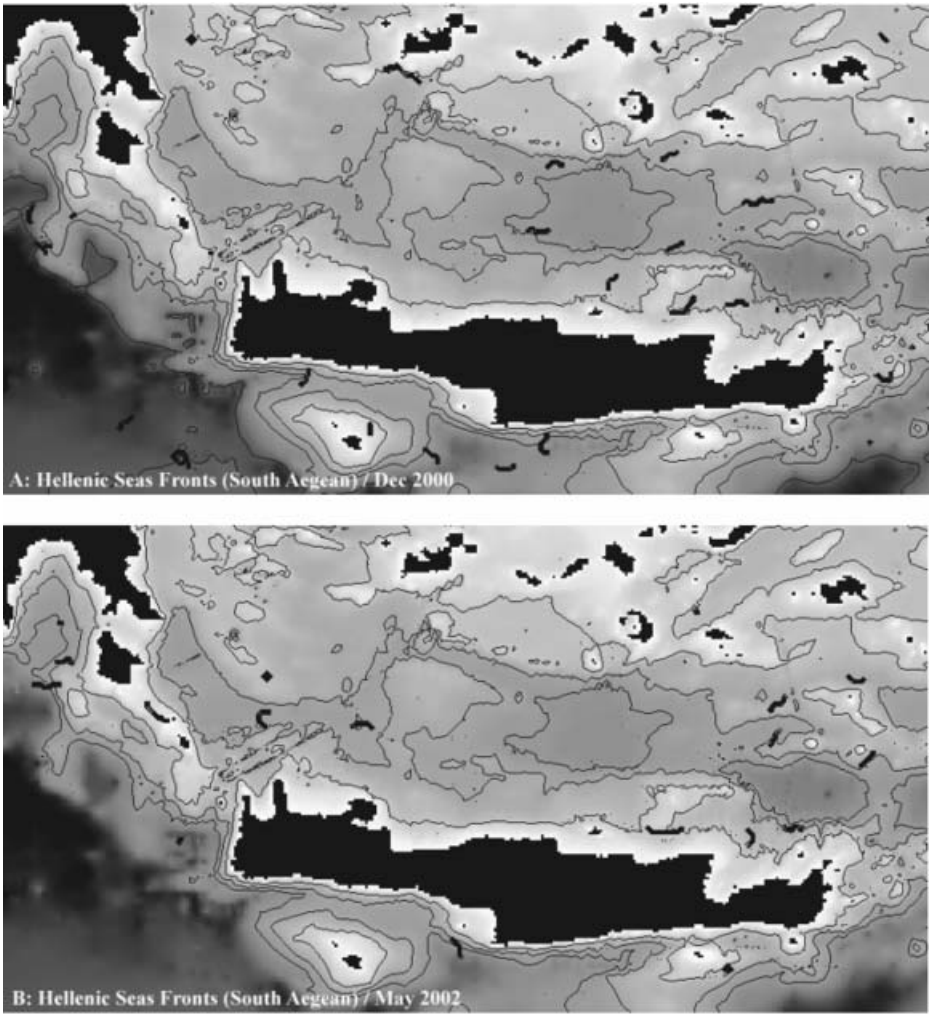


Figure 4. Front and isobath associations in the South Aegean Sea in (A) December 2000 and (B) May 2002. Front/isobath associations are clearly visible around Crete Island.

Specifically, the spatial orientation of mapped shelf and shelf break fronts presents a clearly visible association to the orientation of bathymetric contours (see figures 3–6). The seasonal decomposition for the mean depth of shelf fronts indicates that these fronts appear mostly in deeper waters during winter while they appear in shallower waters during spring and early summer, when increased river runoff and weakened wind patterns are observed in the area (Therianos 1974, Poulos *et al.* 1997). The opposite pattern is observed in the distribution of open water fronts, which seem to follow the seasonal distribution of open water gyre and eddy formations (Theocharis *et al.* 1999, Larnicol *et al.* 2002).

Relationships between the variability of measured maximum sustained wind speed (in terms of standard deviation) with the number of mapped fronts in the North Aegean Sea give statistically significant results (see figures 7 and 8). The Spearman's correlation function gives a statistically significant ($p=0.0001$) coefficient for these two samples of $r=0.411$. The linear regression model between

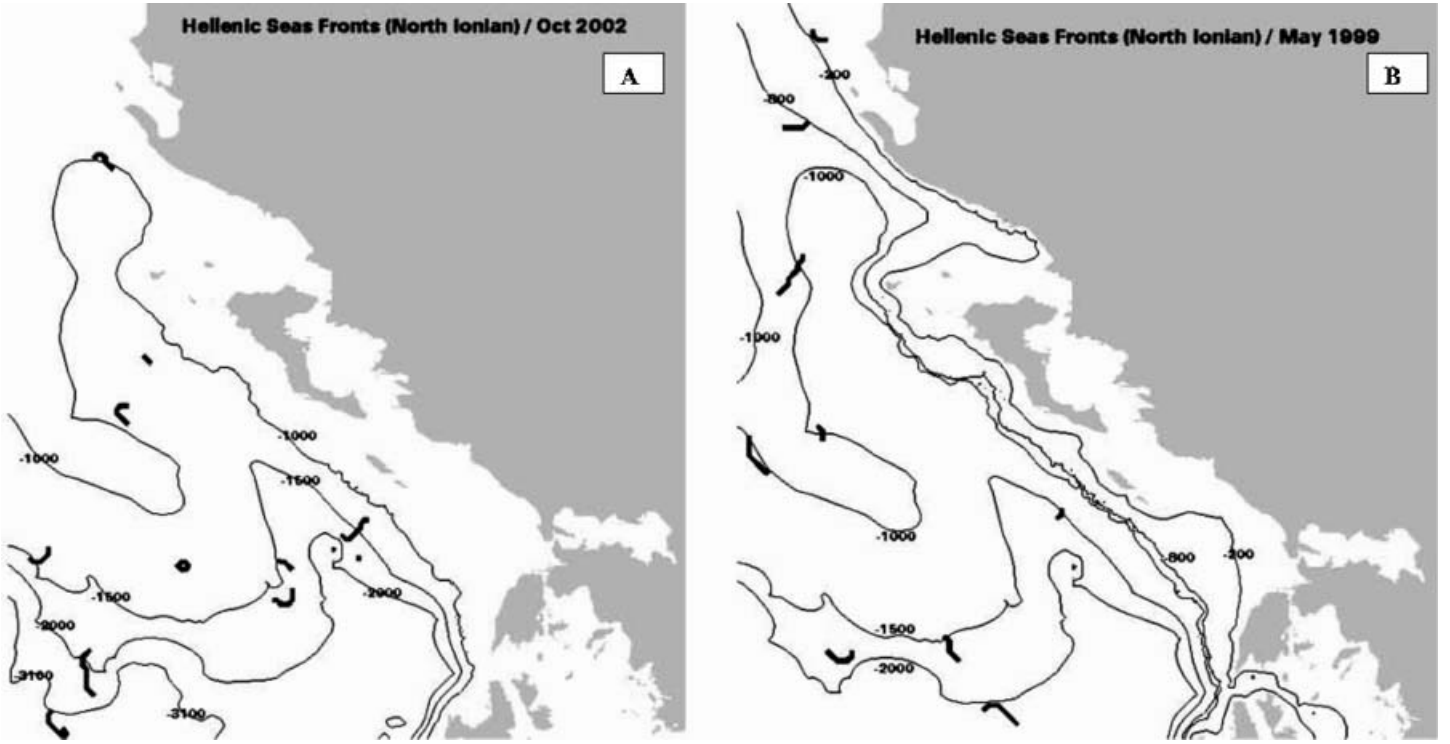


Figure 5. Front and isobath associations in the North Ionian Sea in (A) October 2002 and (B) May 1999. Front to isobath associations are clearly visible offshore Corfu Island.

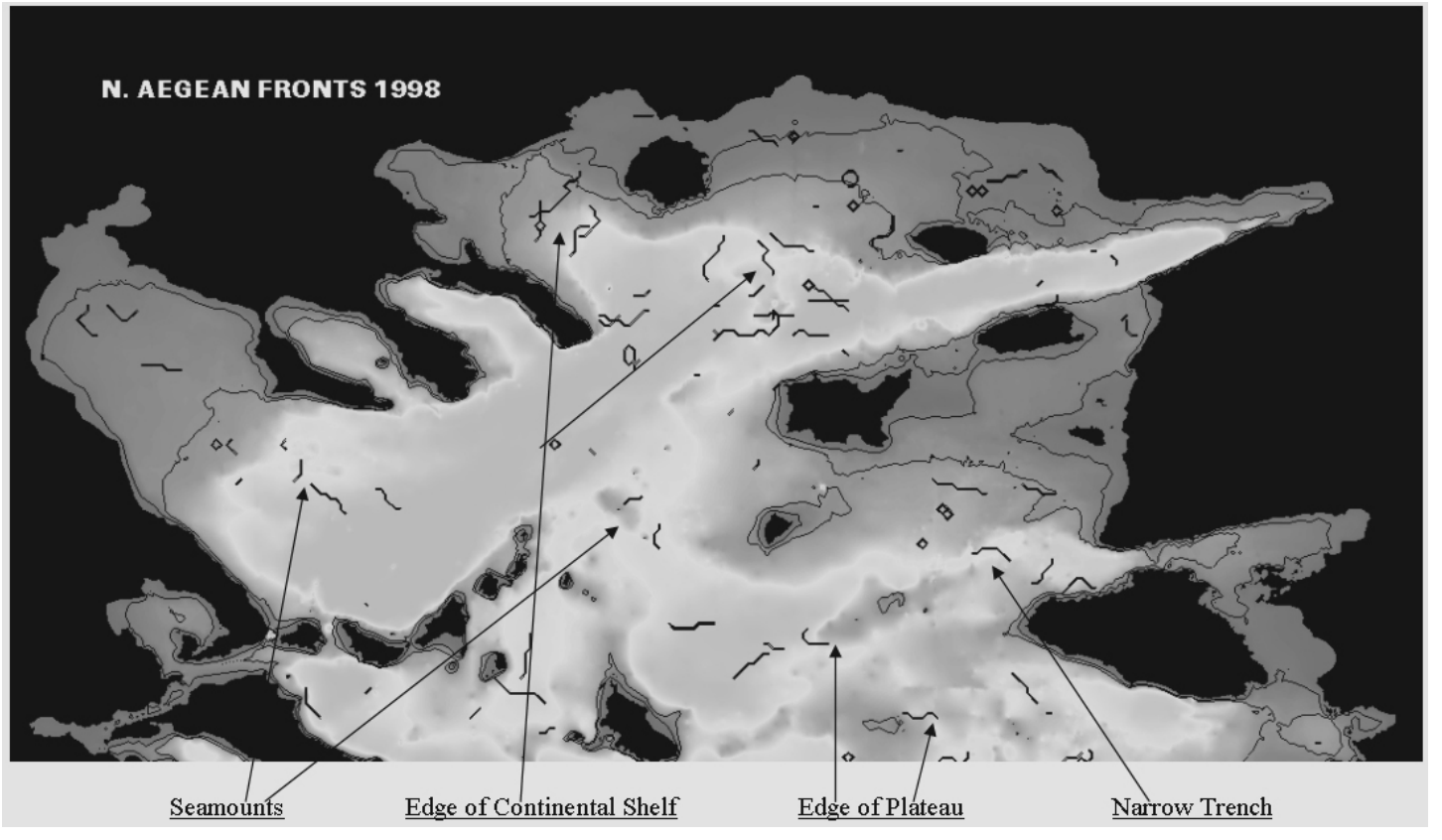


Figure 6. Yearly front spatial associations to various bottom topographic features (seamounts, edge of continental shelf, edge of plateau, narrow trenches) in the North Aegean Sea during 1998. Isobaths of 50 m and 100 m are also shown (grey scale: dark grey to light grey for shallow to deeper regions).

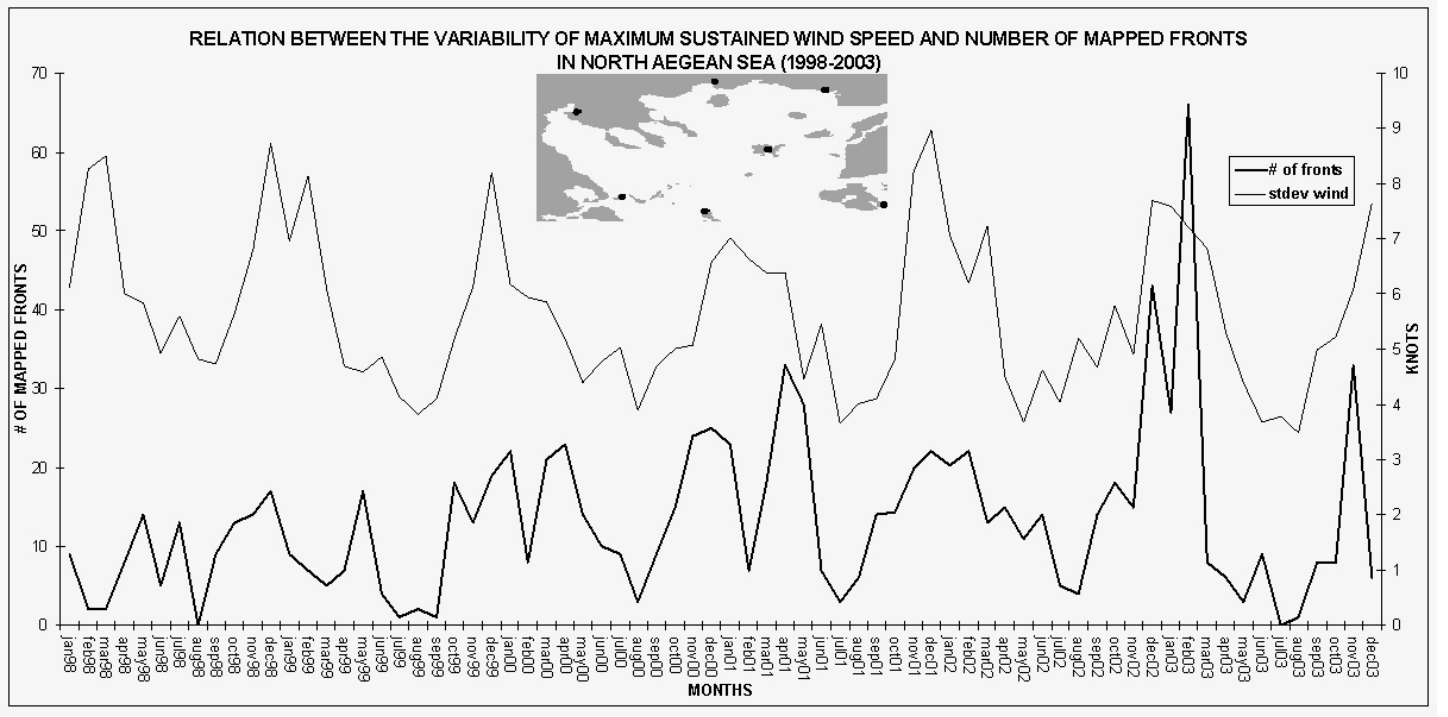


Figure 7. Relationship between the variability of measured maximum sustained wind speed (in terms of standard deviation: thin line) with the number of mapped fronts (thick line) in the North Aegean Sea (Spearman's $r=0.411$, $p=0.0001$ and linear regression model adjusted $r^2=0.66$, $p=0.0001$). The small map shows the location of wind stations.

Table 1. Monthly and seasonal mean environmental characteristics of shelf, shelf break and open water mesoscale thermal fronts in the Hellenic Seas (Eastern Mediterranean Sea) during 1998–2003.

| | Shelf fronts (coast to −350m) | | | | Shelf break fronts (−350m to −650m) | | | | Open water fronts (deeper than −650m) | | | |
|---|---|---|---|---|---|---|---|---|---|---|---|---|
| Period 98-03 Month | Mean DSST (°C) | Mean DCHL (mg/m$^3$) | Mean depth (m) | Number of fronts | Mean DSST (°C) | Mean DCHL (mg/m$^3$) | Mean depth (m) | Number of fronts | Mean DSST (°C) | Mean DCHL (mg/m$^3$) | Mean depth (m) | Number of fronts |
| Jan | −1.10 | 0.6199 | −177 | 10 | −0.94 | 0.1439 | −508 | 8 | −0.75 | 0.0943 | −2520 | 58 |
| Feb | −0.93 | 0.3163 | −201 | 11 | −0.66 | 0.3848 | −510 | 8 | −0.66 | 0.0900 | −2524 | 57 |
| Mar | −0.73 | 0.2709 | −207 | 9 | −0.52 | 0.1432 | −467 | 4 | −0.53 | 0.0710 | −2502 | 56 |
| Apr | −0.97 | 0.7103 | −182 | 10 | −0.78 | 0.1092 | −477 | 7 | −0.53 | 0.0718 | −2492 | 56 |
| May | −1.63 | 0.1675 | −167 | 9 | −0.88 | 0.1551 | −498 | 7 | −0.57 | 0.0552 | −2423 | 50 |
| Jun | −0.80 | 0.1928 | −190 | 5 | −0.75 | 0.0915 | −456 | 3 | −0.37 | 0.0485 | −2554 | 28 |
| Jul | −0.35 | 0.1135 | −150 | 2 | −0.48 | 0.1726 | −477 | 2 | −0.26 | 0.0543 | −2788 | 17 |
| Aug | −0.36 | 0.1472 | −138 | 3 | −0.49 | 0.1782 | −493 | 2 | −0.29 | 0.0456 | −2712 | 20 |
| Sep | −0.46 | 0.3292 | −185 | 3 | −0.43 | 0.1232 | −514 | 4 | −0.43 | 0.0588 | −2577 | 35 |
| Oct | −0.80 | 0.1604 | −177 | 6 | −0.52 | 0.0942 | −518 | 7 | −0.61 | 0.0643 | −2415 | 48 |
| Nov | −0.92 | 0.2243 | −178 | 13 | −0.79 | 0.2178 | −488 | 10 | −0.80 | 0.0735 | −2593 | 55 |
| Dec | −0.96 | 0.2709 | −199 | 15 | −0.95 | 0.1670 | −491 | 11 | −1.09 | 0.1131 | −2452 | 80 |
| All month | −0.83 | 0.2936 | −179 | 8 | −0.68 | 0.1651 | −491 | 6 | −0.57 | 0.0700 | −2546 | 47 |
| Win | −0.92 | 0.4023 | −195 | 10 | −0.71 | 0.2240 | −495 | 7 | −0.65 | 0.0851 | −2515 | 57 |
| Spr | −1.13 | 0.3569 | −180 | 8 | −0.80 | 0.1186 | −477 | 5 | −0.49 | 0.0585 | −2490 | 45 |
| Sum | −0.39 | 0.1966 | −158 | 3 | −0.46 | 0.1547 | −497 | 3 | −0.33 | 0.0529 | −2692 | 24 |
| Fal | −0.89 | 0.2185 | −185 | 11 | −0.75 | 0.1597 | −499 | 10 | −0.83 | 0.0836 | −2487 | 61 |

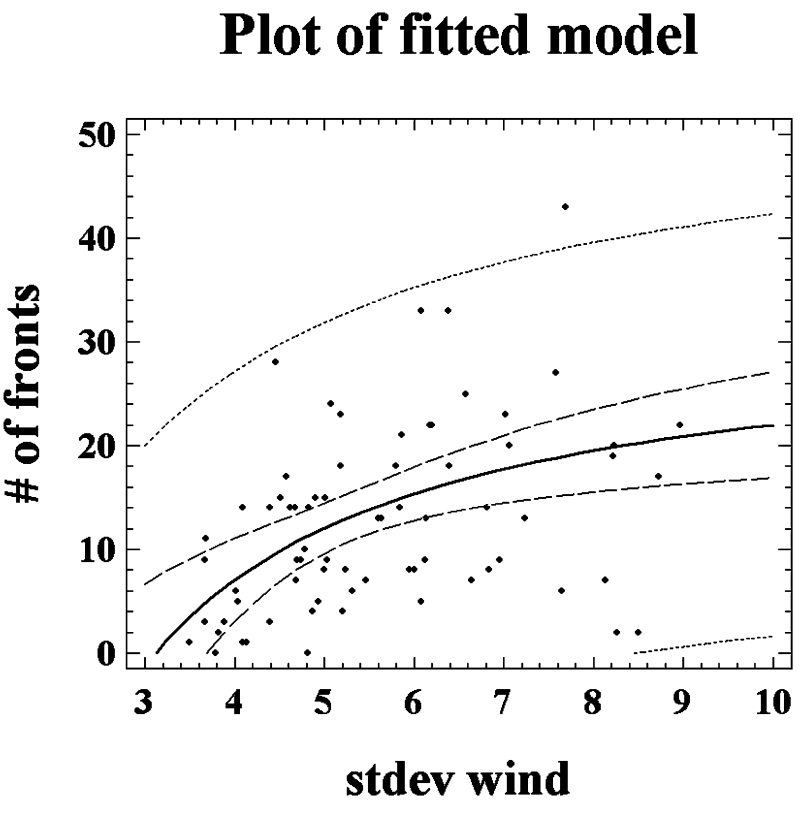


Figure 8. Linear regression model (reciprocal X model) describing the relationship of the variability of maximum sustained wind speed to the number of mapped thermal fronts in the North Aegean Sea.

the two variables gives an adjusted $r^2=0.66$ ($p=0.0001$), which means that the 66% of the variability of the number of mapped fronts can be explained by the standard deviation of the maximum sustained wind speed. The variability of maximum sustained wind speed during 1998–2003 along with the bottom topography (extensive continental shelf followed by a deep trench with distributed seamounts) is adequate to trigger frontal system formations.

From a physical oceanography perspective, the numbers of coastal and offshore fronts reveal an annual periodicity with a decrease during summer. The same periodicity applies to the shelf break fronts but with a slightly differentiated pattern since apart from the decreased number of fronts observed during summer, there is an abrupt decrease of the number of fronts in March. This may be attributed to the fact that in the Mediterranean Sea, March and October are the transition months from summer to winter (Larnicol *et al*. 2002). During summer, the homogeneously stratified water column of the Aegean Sea is influenced by the Etesian winds resulting in heterogeneous SST distribution during winter (Christopoulos 1997). Thus, the maximum number of mapped fronts is, in all three front types, recorded in December (see table 1).

A comparison of the mean DSST of all types of fronts points out a significant difference between the medians during 1998–2003 (Kruskall-Wallis test, $p=0.0058$), with coastal fronts presenting the higher median DSST (in absolute value). The

pattern revealed by time series analysis of the shelf fronts mean DSST indicates a decrease of the absolute DSST value during summer but also an abrupt fall in March and a peak in May. A less sharp pattern is revealed by mean DSST in offshore fronts with a relatively small decline in March, a minimum in July and a maximum value in December. The mean DSST values in shelf break fronts appear to be a random time series indicating that the causative force of the strength of advection of water masses is related to topographic features (bathymetry). Similarly, a significant statistical difference between the mean DCHL of all types of fronts is apparent when comparing the medians ($p=3.94\cdot10^{-11}$), showing an increase in DCHL from open water to shelf break and shelf fronts (see table 1 and figure 9).

The application of the proposed sink method on SST lattice data arrays with adequate resolution provides front occurrence maps with great detail on the length and shape of mesoscale thermal fronts. Based on the generally accepted hypothesis that frontal zones support increased zooplankton populations (Bakun 1996), the selection of spatially connected sink cells, characterized by both negative DSST and positive DCHL pattern (thermal fronts), excludes sinks that may be assumed as patches of cold surface water (e.g. sinks associated to negative DCHL patterns). The per cent of identified sink regions that are characterized by positive DCHL (thermal fronts) is 76% (1998), 71% (1999), 66% (2000), 68% (2001), 64% (2002 and 2003), averaged at 68% for the study period.

A comparison of the sink method to other widely accepted methods for automated edge-detection of fronts (e.g. gradient and histogram methods) reveals that the main difference is on the scale of resulted mapped fronts. On a mesoscale level and leaving aside the spatial resolution of input images, results of the gradient and histogram methods depend on the targeted scale of fronts (e.g. some spatially small or weak fronts may not be detected). In gradient and histogram methods, gradient coefficients or threshold values must be applied, respectively (Ullman and Cornillon 2000). Results of the proposed sink method depend only on the spatial resolution of the input images. The proposed method detects even the weakest thermal discontinuities because it flags all those pixels that present a change (weak or strong drop in SST) when they are compared to immediate neighbouring image cells without application of gradient coefficients or threshold values.

The distribution of mesoscale thermal fronts, derived through the proposed sink method, presents a clear spatial association with bathymetric contours and follows the general oceanographic patterns in the area (relatively homogeneous stratification during late spring and summer that is interrupted by Etesian energy, which is transferred through fall and winter, resulting in heterogeneous stratification). Wind patterns in the North Aegean Sea (generally northerly winds throughout the year interrupted by southerly winds during sporadic periods in autumn) appear adequate to initiate frontal systems formation in the area.

## 4. Conclusion

A new method for the identification and mapping of mesoscale transient thermal fronts was presented. The 'sink' method is a set of GIS routines that handle thermal fronts as data value sinks in SST lattice data arrays. This new method complements the two main methods of using SST satellite data for automated edge-detection of fronts, the histogram and the gradient algorithm methods, with the difference that it targets mesoscale transient features (no gradient coefficients or threshold values applied) while automated edge-detection methods

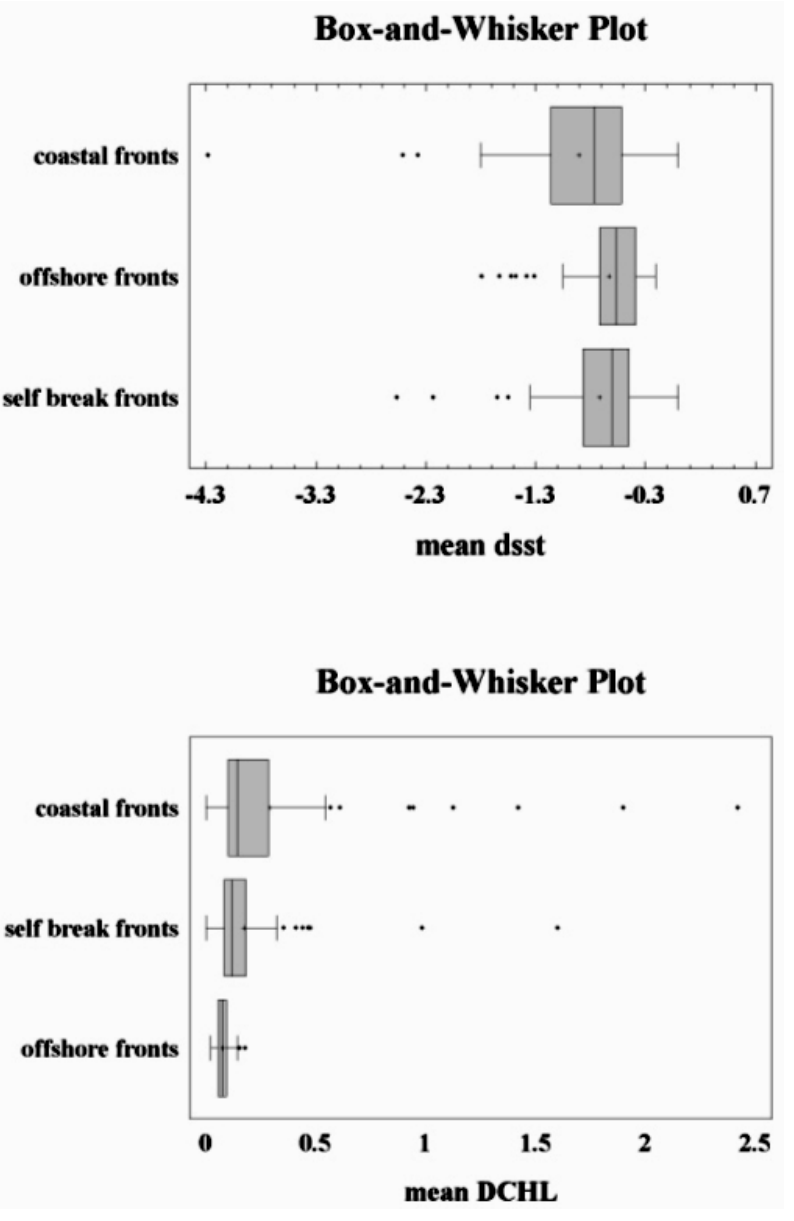


Figure 9. Box-and-Whisker plots comparing DSST and DCHL values among coastal, shelf-break and offshore fronts in the Hellenic Seas.

mainly target spatially larger permanent features (with gradient coefficients or threshold values applied).

Front occurrence maps resulting from the application of the proposed sink method on historical and real-time SST and CHL imagery may be used for the identification of persistent high productivity frontal regions as well as for aiding local fishing fleets to identify certain operation areas for short periods (daily or weekly). Future work will include the analysis of front distribution in relation to persistent marine productivity hotspots in the Eastern Mediterranean along with

small and large pelagic, commercially important resources in the area (sardine, anchovy, squid and tuna). Results from such studies will allow us to make thermal fronts maps available to local fishing fleets and obtain feedback information from fishermen on the effectiveness of model output.

Finally, the application of GIS technology in the development of the 'sink' method proved ideal for the full exploration and mapping of mesoscale transient oceanic processes derived from remotely sensed data.

**Acknowledgements**

This work was partly funded by a European Communities (Fifth Framework Programme) research project (CEPHSTOCK QOL-2001-5.1.2) and a Hellenic Secretariat of Research and Technology (Ministry of Development) project (IMAS E2050-5/1). The authors thank the SeaWiFS Project and the Distributed Active Archive Centre at the Goddard Space Flight Centre, Greenbelt, MD 20771, for the production and distribution of SeaWIFS data, the German Aerospace Agency for the distribution of AVHRR data as well as two anonymous referees for constructive comments on the manuscript.

**References**

ACHA, E.M., MIANZAN, H.W., GUERRERO, R.A., FAVERO, M. and BAVA, J., 2004, Marine fronts at the continental shelfs of austral South America: Physical and ecological processes. *Journal of Marine Systems*, **44**, pp. 83–105.

AGOSTINI, V.N. and BAKUN, A., 2002, 'Ocean triads' in the Mediterranean Sea: Physical mechanisms potentially structuring reproductive habitat suitability (with example application to European anchovy, *Engraulis encrasicolus*). *Fisheries Oceanography*, **11**, pp. 129–142.

ALLEN, J.T., SMEED, D.A., TINTORE, J. and RUIZ, S., 2001, Mesoscale subduction at the Almeria-Oran front: Part 1: Ageostrophic flow. *Journal of Marine Systems*, **30**, pp. 263–285.

BAKUN, A., 1996, *Patterns in the Ocean - Ocean Processes and Marine Population Dynamics*, pp. 156–168 (La Jolla: California Sea Grant College System).

BELKIN, I.M., 2002, New challenge: Ocean fronts. *Journal of Marine Systems*, **37**, pp. 1–2.

BELKIN, I.M. and GORDON, A.L., 1996, Southern Ocean fronts from the Greenwich meridian to Tasmania. *Journal of Geophysical Research*, **101**, pp. 3675–3696.

BONATTI, J.P. and RAO, V.B., 1999, Meso-scale perturbations and thermocline fronts in the south Atlantic Ocean. *Dynamics of Atmospheres and Oceans*, **30**, pp. 1–24.

BORZELLI, G. and LIGI, R., 1999, Autocorrelation scales of the SST distribution and water masses stratification in the Channel of Sicily. *Journal of Atmospheric and Oceanic Technology*, **16**, pp. 776–781.

CAYULA, J.F. and CORNILLON, P., 1992, Edge detection algorithm for SST images. *Journal of Atmospheric and Oceanic Technology*, **9**, pp. 67–80.

CAYULA, J.F. and CORNILLON, P., 1995, Multi-image edge detection for SST images. *Journal of Atmospheric and Oceanic Technology*, **12**, pp. 821–829.

CHRISTOPOULOS, S., 1997, Wind-wave modelling aspects within complicate topography. *Annales Geophysicae*, **15**, pp. 1340–1353.

ESRI, 1994, *ARC Macro Language* (Redlands: Environmental Systems Research Institute Press).

FELIKS, Y. and GHIL, M., 1993, Downwelling-front instability and eddy formation in the Eastern Mediterranean. *Journal of Physical Oceanography*, **23**, pp. 61–78.

FERRIER, G. and ANDERSON, J.M., 1997, The application of remotely sensed data in the study of frontal systems in the Tay Estuary, Scotland, U.K. *International Journal of Remote Sensing*, **18**, pp. 2035–2065.

FIELDING, S., CRISP, N., ALLEN, J.T., HARTMAN, M.C., RABE, B. and ROE, H.S.J., 2001, Mesoscale subduction at the Almeria-Oran front: Part 2. Biophysical interactions. *Journal of Marine Systems*, **30**, pp. 287–304.

HICKOX, R., BELKIN, I., CORNILLON, P. and SHAN, Z., 2000, Climatology and seasonal variability of ocean fronts in the East China, Yellow and Bohai Seas from satellite SST data. *Geophysical Research Letters*, **27**, pp. 2945–2948.

KOSTIANOY, A.G., GINZBURG, A.I., FRANKIGNOULLE, M. and DELILLE, B., 2004, Fronts in the Southern Indian Ocean as inferred from satellite sea surface temperature data. *Journal of Marine Systems*, **45**, pp. 55–73.

LARNICOL, G., AYOUB, N. and LE TRAON, P.Y., 2002, Major changes in Mediterranean sea level variability from 7 years of TOPEX/Poseidon and ERS-1/2 data. *Journal of Marine Systems*, **33–34**, pp. 63–89.

LEGECKIS, R., BROWN, C.W. and CHANG, P.S., 2002, Geostationary satellites reveal motions of ocean surface fronts. *Journal of Marine Systems*, **37**, pp. 3–15.

L'HELGUEN, S., LE CORRE, P., MADEC, C. and MORIN, P., 2002, New and regenerated production in the Almeria-Oran front area, eastern Alboran Sea. *Deep Sea Research I*, **49**, pp. 83–99.

MALAKOFF, D., 2004, New tools reveal treasures at ocean hot spots. *Science*, **304**, pp. 1104–1105.

MathSoft, 1999, *S-Plus 2000 Guide to Statistics, Volume 1* (Seattle: MathSoft Data Analysis Products Division).

MAVOR, T.P. and BISAGNI, J.J., 2001, Seasonal variability of sea-surface temperature fronts on Georges Bank. *Deep Sea Research II*, **48**, pp. 215–243.

MESICK, S.M., BOODA, M.H. and GIBSON, B.A., 1998, Automated detection of oceanic fronts and eddies from remotely sensed satellite data using ArcInfo grid processing. In *18th Annual ESRI International User Conference*, 27–31 July 1998, San Diego, CA (Redlands: ESRI Press), p. 252.

MILLER, P., 2004, Multi-spectral front maps for automatic detection of ocean colour features from SeaWiFS. *International Journal of Remote Sensing*, **25**, pp. 1437–1442.

NARDELLI, B.B., SANTOLERI, R. and SPARNOCCHIA, S., 2001, Small mesoscale features at a meandering upper-ocean front in the Western Ionian Sea (Mediterranean Sea): Vertical motion and potential vorticity analysis. *Journal of Physical Oceanography*, **31**, pp. 2227–2250.

POULOS, S.E., DRAKOPOULOS, P.G. and COLLINS, M.B., 1997, Seasonal variability in sea surface oceanographic conditions in the Aegean Sea (Eastern Mediterranean): An overview. *Journal of Marine Systems*, **13**, pp. 225–244.

SABATES, A., SALAT, J. and MASO, M., 2004, Spatial heterogeneity of fish larvae across a meandering current in the northwestern Mediterranean. *Deep Sea Research I*, **51**, pp. 545–557.

SHAW, A.G.P. and VENNELL, R., 2000, A front-following algorithm for AVHRR SST imagery. *Remote Sensing of Environment*, **72**, pp. 317–327.

SHAW, A.G.P. and VENNELL, R., 2001, Measurements of an oceanic front using a front-following algorithm for AVHRR SST imagery. *Remote Sensing of Environment*, **75**, pp. 47–62.

THEOCHARIS, A., BALOPOULOS, E., KIOROGLOU, S., KONTOYIANNIS, H. and IONA, A., 1999, A synthesis of the circulation and hydrography of the South Aegean Sea and the Straits of the Cretan Arc (March 1994–January 1995). *Progress in Oceanography*, **44**, pp. 469–509.

THERIANOS, A.D., 1974, Rainfall and geographical distribution of river runoff in Greece. *Bulletin of the Geological Society of Greece*, **11**, pp. 28–58.

ULLMAN, D.S. and CORNILLON, P.C., 1999, Surface temperature fronts off the East Coast of North America from AVHRR imagery. *Journal of Geophysical Research*, **104**, pp. 23459–23478.

ULLMAN, D.S. and CORNILLON, P.C., 2000, Evaluation of front detection methods for satellite-derived SST data using in situ observations. *Journal of Atmospheric and Oceanic Technology*, **17**, pp. 1667–1675.

ULLMAN, D.S. and CORNILLON, P.C., 2001, Continental shelf surface thermal fronts in winter off the northeast U.S. coast. *Continental Shelf Research*, **21**, pp. 1139–1156.

VALAVANIS, V.D., 2002, *Geographic Information Systems in Oceanography and Fisheries*, pp. 74–78 (London: Taylor & Francis).

VALAVANIS, V.D., KATARA, I. and PALIALEXIS, A., 2004, Critical regions: A GIS-based modeling approach for the mapping of marine productivity hotspots. *Aquatic Sciences*, **36**, pp. 234–243.

VELEGRAKIS, A.F., OIKONOMOU, E., THEOCHARIS, A., COLLINS, M.B., KONTOYIANNIS, H., PAPADOPOULOS, V., VOULGARIS, G., WELLS, T. and BALOPOULOS, E., 1999, Internal waves revealed by Synthetic Aperture Radar (SAR) imagery in the vicinity of the eastern Cretan Arc Straits (Eastern Mediterranean). *Progress in Oceanography*, **44**, pp. 553–572.

WALUDA, C.M., RODHOUSE, P.G., TRATHAN, P.N. and PIERCE, G.J., 2001, Remotely sensed mesoscale oceanography and the distribution of *Illex argentinus* in the South Atlantic. *Fisheries Oceanography*, **10**, pp. 207–216.